Cell Communication and Signaling

RESEARCH

Open Access

MYO6 contributes to tumor progression and enzalutamide resistance in castration-resistant prostate cancer by activating the focal adhesion signaling pathway

Shengfeng Zheng[1,2,3,6†], Zhe Hong[1,2,3*†], Yao Tan[1,2,4†], Yue Wang[1,2,3], Junhong Li[1,2,3], Zihao Zhang[1,2,3], Tao Feng[1,2,3], Zongyuan Hong[5*], Guowen Lin[1,2,3*] and Dingwei Ye[1,2,3*]

Abstract

Background Enzalutamide (Enz) resistance is a poor prognostic factor for patients with castration-resistant prostate cancer (CRPC), which often involves aberrant expression of the androgen receptor (AR). Myosin VI (MYO6), one member of the myosin family, plays an important role in regulating cell survival and is highly expressed in prostate cancer (PCa). However, whether MYO6 is involved in Enz resistance in CRPC and its mechanism remain unclear.

Methods Multiple open-access databases were utilized to examine the relationship between MYO6 expression and PCa progression, and to screen differentially expressed genes (DEGs) and potential signaling pathways associated with the MYO6-regulated Enz resistance. Both in vitro and in vivo tumorigenesis assays were employed to examine the impact of MYO6 on the growth and Enz resistance of PCa cells. Human PCa tissues and related clinical biochemical data were utilized to identify the role of MYO6 in promoting PCa progression and Enz resistance. The molecular mechanisms underlying the regulation of gene expression, PCa progression, and Enz resistance in CRPC by MYO6 were investigated.

Results MYO6 expression increases in patients with PCa and is positively correlated with AR expression in PCa cell lines and tissues. Overexpression of AR increases MYO6 expression to promote PCa cell proliferation, migration and invasion, and to inhibit PCa cell apoptosis; whereas knockdown of MYO6 expression reverses these outcomes and enhances Enz function in suppressing the proliferation of the Enz- sensitive and resistant PCa cells both in vitro and in

†Shengfeng Zheng, Zhe Hong, and Yao Tan contributed equally to this work.

*Correspondence:
Zhe Hong
hz_urology@shca.org.cn
Zongyuan Hong
zyhong@wnmc.edu.cn
Guowen Lin
guowenlin@urocancer.org
Dingwei Ye
dwyeli@163.com

Full list of author information is available at the end of the article

© The Author(s) 2024. **Open Access** This article is licensed under a Creative Commons Attribution-NonCommercial-NoDerivatives 4.0 International License, which permits any non-commercial use, sharing, distribution and reproduction in any medium or format, as long as you give appropriate credit to the original author(s) and the source, provide a link to the Creative Commons licence, and indicate if you modified the licensed material. You do not have permission under this licence to share adapted material derived from this article or parts of it. The images or other third party material in this article are included in the article's Creative Commons licence, unless indicated otherwise in a credit line to the material. If material is not included in the article's Creative Commons licence and your intended use is not permitted by statutory regulation or exceeds the permitted use, you will need to obtain permission directly from the copyright holder. To view a copy of this licence, visit http://creativecommons.org/licenses/by-nc-nd/4.0/.

vivo. Mechanistically, AR binds directly to the promoter region (residues − 503 to − 283 base pairs) of *MYO6* gene and promotes its transcription. Furthermore, MYO6 activates focal adhesion kinase (FAK) phosphorylation at tyrosine-397 through integrin beta 8 (ITGB8) modulation to promote PCa progression and Enz resistance. Notably, inhibition of FAK activity by Y15, an inhibitor of FAK, can resensitize CRPC cells to Enz treatment in cell lines and mouse xenograft models.

Conclusions MYO6 has pro-tumor and Enz-resistant effects in CRPC, suggesting that targeting MYO6 may be beneficial for ENZ-resistant CRPC therapy through the AR/MYO6/FAK signaling pathway.

Keywords Myosin VI, Enzalutamide resistance, Androgen receptor, Castration-resistant prostate cancer, Y15

Introduction

Androgen deprivation therapy (ADT) is the primary treatment for patients with advanced metastatic prostate cancer (mPCa) and the basis for various novel combination therapy regimens [1]. However, in most patients, the disease progresses to castration-resistant prostate cancer (CRPC) within approximately 2–3 years after initial ADT treatment [2]. Currently, potent next-generation inhibitors targeting androgen signaling, such as enzalutamide (Enz) and abiraterone, are approved by the US Food and Drug Administration (FDA) for the treatment of CRPC [3]. Unfortunately, resistance to these drugs occurs in most patients, which means that no effective treatment is available for CRPC patients. Therefore, new strategies for reducing drug resistance to next-generation androgen receptor (AR)-targeted therapy and means of improving the prognosis of CRPC patients need to be explored.

Accumulating evidence has indicated that progression to advanced drug-resistant CRPC involves multiple molecular mechanisms correlated with irregular AR signaling [4, 5]. Several factors related to the dysregulated AR signaling have been verified, including AR hypersensitivity corresponding to excessive AR gene amplification, AR mutations in the ligand-binding domain (LBD) or splicing variants (e.g. AR-variant 7 [AR-V7]) [6], altered function and expression of AR coregulators [7], and overexpression of AR expression via aberrant epigenetic modifications. In addition, other alternative AR-independent or AR-bypass pathways, including inactivation or loss of expression of tumor suppressor genes (e.g., phosphatase and tensin homologue deleted on chromosome ten [PTEN], tumor protein 53 [TP53], and retinoblastoma gene [RB1]) [8] and activation of antiapoptosis genes (e.g., B-cell lymphoma-2 [BCL-2]), also participate in CRPC procession [9]. The irregular AR signaling in recurrently metastatic CRPC patients often indicates invalid Enz treatment [6, 10]. The mechanisms and context underlying the role of irregular AR-induced Enz treatment failure and the options available to antagonize this resistance mechanism have not been fully elucidated.

Myosins constitute a protein superfamily of more than 18 known members and are the main motor proteins that transport cargos along actin filaments using the energy derived from ATP hydrolysis [11, 12]. Myosin VI (MYO6), a unique member of the myosin family that moves towards the minus end of actin filaments, has been suggested to play an important role in regulating cell survival [13, 14]. Cho et al. [15] reported that p53 or DNA damage caused in a p53-dependent manner alters the intracellular location of MYO6, and knockdown of MYO6 expression renders cells susceptible to apoptosis. Previous reports have indicated that MYO6 is overexpressed in aggressive cancers including ovarian and breast, and depletion of MYO6 leads to decreased cell motility and/or proliferation [14, 16]. MYO6 is also highly expressed in PCa [17, 18], and suppression of MYO6 expression reduces migration and colony formation by decreasing the phosphorylation of proline-rich Akt substrate 40 (PRAS40) and extracellularly regulated protein kinase 1/2 (ERK1/2) in vitro [19]. However, whether MYO6 is involved in Enz resistance in CRPC and its mechanism remain unclear.

Here, we reported that MYO6 expression was positively correlated with AR expression and was higher in the 22Rv1, LNCaP, C4-2, C4-2B, and Enz-resistant (C4-2R) cell lines rather than in the AR negative cells including DU145 and PC-3. Overexpression of AR promoted PCa cell proliferation, migration, and invasion; whereas knockdown of MYO6 expression reversed these outcomes and enhanced the sensitivity of 22Rv1, LNCaP, C4-2, and C4-2R cells to Enz treatment, and this phenomenon was also observed by supplementation with the focal adhesion kinase (FAK) inhibitor Y15 in vitro and in vivo. Mechanistically, AR binds directly to the *MYO6* gene and promotes its transcription. Furthermore, MYO6 activates focal adhesion kinase (FAK) phosphorylation at tyrosine-397 (Y397) to strengthen the process of epithelial mesenchymal transition (EMT) through the promotion of snail1, vimentin, and N-cadherin expression; decreases E-cadherin expression; and inhibits cell apoptosis by upregulating BCL-2 expression, thus promoting PCa progression and Enz resistance. Overall, we identified a novel AR/MYO6/FAK axis in which MYO6 acts as an AR target, contributing to tumor progression and enzalutamide resistance in PCa, which could lead to

potential therapeutic options targeting MYO6 to overcome Enz resistance in CRPC.

Materials and methods

Sample collection

A total 25 pairs of Human prostate carcinoma tissues and adjacent normal tissues were obtained from patients who underwent radical prostatectomy at the Shanghai Cancer Center affiliated with Fudan University during 2021 to 2022. Related clinical biochemical data were collected from the medical records. Tissues 2 cm from the tumor edge were used as adjacent controls. Histopathological assessment was carried out blindly by two senior pathologists. The tissues were stored at -80 °C until further investigation. All experiments of human tissues and clinical biochemical data in this study were approved by the Ethics Committee of FUSCC, following the Declaration of Helsinki, and written informed consent was obtained from each patient.

Cell lines and cell culture conditions

PCa cell lines (22Rv1, DU145, LNCaP, PC-3, C4-2, and C4-2B) and the benign prostatic epithelial cell line RWPE-1 were purchased from the Chinese Academy of Science (CAS) or American Type Culture Collection (ATCC). These PCa cell lines were cultured in RPMI 1640 medium supplemented with 10% fetal bovine serum (FBS; Gibco) and 1% penicillin–streptomycin solution. RWPE-1 cells were cultured in keratinocyte serum-free medium. Enz-resistant C4-2 (C4-2R) cells were generated by treating C4-2 CRPC cells with whole medium containing a series of concentrations of Enz (from 10 μM to 30 μM) until the cells were no longer sensitive to Enz [20], and then the C4-2R cells were maintained in medium supplemented with 20 μM Enz for experiments. The human embryonic kidney cell line 293T was also obtained from CAS and cultured in DMEM supplemented with 10% FBS. All cells were cultured in a humidified incubator with 5% CO_2 at 37 °C. In this study, all the cells were authenticated, and regular mycoplasma testing was performed to avoid the use of mycoplasma-contaminated cells.

Plasmid construction and cell transfection

Plasmid delivery was conducted using Lipofectamine 3000 (Invitrogen) according to the manufacturer's instructions. The targeted shRNA was ligated into the pLKO.1 vector as described previously [21]. The MYO6 and AR overexpression plasmids were purchased from GeneCopoeia. The plasmids above, together with the lentiviral packaging system (psPAX2 and pMD2G), were cotransfected into 293T cells for 48 h to produce the lentivirus particle mixture. The cells were collected in 15 mL centrifuge tubes after filtration through a 0.45 μM filter tip and were subsequently incubated with the appropriated PCa cells. The primers used are listed in Table S1.

Immunohistochemistry (IHC)

Fresh prostate tissues were embedded in paraffin after fixation in 4% formaldehyde for 12 h and cut into 4 μM thick sections. After blocking with goat serum for 15 min, the tissues were incubated with primary antibodies against MYO6 (Proteintech, 1:200) for 12 h at 4 °C. After washing 3 times with phosphate-buffered saline (PBS), the tissues were incubated with a secondary horseradish peroxidase (HRP)-conjugated goat antibody against rabbit IgG (Proteintech, 1:1000). Nonimmune serum from the same species was used as a negative control. Immunoreactivity scores based on staining intensity and the proportion of stained cells were calculated. The staining intensity was scored as follows: 0=negative; 1=weak; 2=moderate; and 3=strong. The ratio of stained cells was estimated as follows: null=0; 1–10% = 1; 11–50% = 2; 51–80% = 3; and >80% = 4. The immunoreactivity score was obtained by the intensity score, which was calculated as the ratio of the staining score to the total score. The antibodies used are listed in Table S2.

Western blot analysis

Briefly, tissues or cell protein lysates were extracted by adding RIPA lysis and extraction buffer (Solarbio) supplemented with 1% protease and phosphatase inhibitor cocktail. A total of 20 μg of protein per sample was separated via a 10% SDS–PAGE gel and transferred to 0.22 μm PVDF membranes (Millipore). After blocking with 5% nonfat milk for 1 h at room temperature, the membranes were incubated with primary antibodies overnight, and the secondary antibodies (Proteintech, 1:10000) were subsequently cross-linked onto the bands. Immunoreactivity was detected using enhanced chemiluminescent autoradiography (YI SHENG). The relative quantity of the protein band was analyzed via ImageJ software. The antibodies used were listed in Table S2.

RNA isolation and RT–qPCR

Total RNA was isolated by using TRIzol reagent (Thermo Scientific). First-strand cDNA was generated from 1 μg of total RNA using the PrimeScript RT Master Mix Perfect Real Time Kit (TaKaRa). RT–qPCR was conducted using a Roche Real-Time System with FastStart Taq DNA Polymerase (Roche). The primers used for RT–qPCR are listed in Table S1. The relative expression of the mRNAs was normalized to the GAPDH expression level, and the $2^{-\Delta\Delta Cet}$ formula was used to calculate the relative mRNA expression.

Cell proliferation assay

A total of 1×10^3 22Rv1, LNCaP, C4-2, or C4-2R cells were seeded into 96-well plates for cell counting kit-8 (CCK-8) assays on days 1, 2, 3, 4, and 5. At various time points, CCK-8 assays were performed by adding 100 μL of fresh medium containing 10 μL of CCK-8 reagent to each well. Enz and/or Y15 were added to the wells on day 1 to investigate treatment efficacy, and an equal volume of DMSO was used as a control. Cell proliferation was determined by reading the absorbance value (optical density, OD) at 450 nm.

Invasion and migration assays

The in vitro invasion assay was performed using a Transwell chamber coated with Matrigel (BD Biosciences), and the migration assay was conducted without Matrigel. After digestion, 3×10^4 LNCaP, 22Rv1, or C4-2 cells were suspended in 200 μL of FBS-free 1640 medium and seeded into the inner chamber, while 500 μL of medium containing 10% FBS was added to the lower chamber. The cells were then cultured in cell incubators for 48 h. The invading cells were fixed with paraformaldehyde and stained with 3% crystal violet solution (Solarbio). Quantification was performed by randomly selecting five visual fields in each group under an optical microscope.

In vitro tumorigenesis assay

We further investigated the role of MYO6 in regulating the tumorigenesis ability of 22Rv1, LNCaP, and C4-2 cells in vitro. A total of 1×10^3 cells were initially cultured in 6-well plates supplemented with 2 mL of medium with 10% FBS. After 10 days, the cells were stained with 3% crystal violet solution (Solarbio). The images were produced by scanning via a cell phone.

Flow cytometry analysis

To investigate cell- cycle distribution and cell apoptosis, flow cytometry with propidium iodide (PI) staining and allophycocyanin-conjugated annexin V and 7-aminoactinomycin D (Vazyme Biotech) were carried out. According to the manufacture's instruction, the PCa cells were washed with PBS and digested with 0.25% EDTA-free trypsin (Gibco). For cell- cycle distribution, approximately 2×10^6 cells were collected and resuspended in a mixture of 1 mL of PI (10 μg/mL) and DNase-free RNase (20 μg/mL) for 20 min. For cell apoptosis assays, the cell density was adjusted to 1×10^5/mL, and the cells were incubated with Annexin V-FITC with PI at room temperature for 25 min. The two kinds of samples were analyzed using a flow cytometer (BD Biosciences) and FlowJo software.

Chromatin immunoprecipitation (ChIP) assay

An EZ-Magna G chromatin immunoprecipitation kit (Millipore, MA, USA) was used for ChIP. After washing with PBS, a total of 1.2×10^7 cells were cross-linked with 4% formaldehyde at room temperature for 10 min, after which the formaldehyde concentration was quenched with 125 mM glycine. The cells were collected in a centrifuge tube via a scraper. The genomic DNA was sonicated to yield fragments ranging from 300 to 1000 bp in length. The lysates were precleared with protein A/G-agarose at 4 °C for 1 h. Primary anti-AR antibody (ab108341, Abcam) or H3K27Ac antibody (ab108341, Abcam) was added to the lysates, which were subsequently incubated on a roller at 4 °C overnight. An IgG antibody (ab171870, Abcam) was used to incubate the cell lysates as a negative control. High-throughput sequencing was conducted on the Illumina HiSeqTM4000 platform. All primitive reads were mapped to the human reference genome of GRCh37/hg19 using Bowtie2 (version 2.1.0) with default configurations [22]. Specific primers targeting protein-binding DNA regions were designed for RT−qPCR to analyze the enrichment rate.

Dual-luciferase assay

After browsing the AR common potential binding sites on JASPAR database (https://jaspar.elixir.no/), several fragments (-2000 to -1, -1822 to -1, -1272 to -1, -1049 to -1, -951 to -1, -503 to -1, and −283 to -1, bp) of the *MYO6* gene promotor were cloned via PCR and ligated into the pGL4.22 luciferase vector. The AR-overexpressing cell line C4-2 and the corresponding control cells were plated in 24-well plates and transfected with the PGL4.22-MYO6- promoter. The pGL4.74 vector was simultaneously transfected as the internal control. Next, the cells were treated with 1 nM dihydrotestosterone (DHT) for 48 h, after which the luciferase activity was measured using a Dual Luciferase Reporter Assay System (Promega, WI, USA) on an HT microplate reader (BioTek, VT, USA) according to the manufacturer's manual.

RNA sequencing (RNA-seq)

RNA-seq of C4-2, C4-2R, and C4-2R-shMYO6 cells was performed by the AZENTA Life Science Center. A total of 1 μg of RNA was treated with DNase I and fragmented using divalent cations and high temperature for cDNA library construction. Then, first-strand cDNA was synthesized with random primers by performing PCR on a hot cycle module. After both ends were repaired, a dA tail was added to the strand in one reaction, and the adaptors were ligated to both ends by T-A ligation. DNA clean beads were subsequently used to perform size selection of adaptor-ligated DNA.

The samples were subsequently amplified via PCR using the P7 and P5 primers, and the PCR products were

validated via agarose gel electrophoresis. According to the manufacturer's instructions, libraries with different indices were composed and finally loaded on an Illumina HiSeq/MGI2000 instrument for sequencing using a 2×150 paired-end (PE) configuration. The primers used are listed in Table S1.

Immunoprecipitation assay

To investigate the interaction between endogenous MYO6 and its target protein, proteins were extracted via lysis buffer and subsequently immunoprecipitated with an anti-MYO6 or anti-FAK antibody (1:100, Abcam). The precipitates were resolved using a 10% SDS–PAGE gel followed by immunoblotting.

Glutathione S-transferase (GST) pull-down assay

Cells were collected and lysed with IP buffer on ice for approximately 40 min. GST fusion proteins were immobilized on glutathione-Sepharose beads (GE Health-care Lifesciences) by incubated at 4 °C for 4 h. After washing with lysis buffer, the beads were incubated with cell lysates at 4 °C overnight. Next the beads were washed six times with washing buffer and resuspended in sample loading buffer and incubated at more than 95 °C for 10 min. The bound protein levels were determined using specific primary antibody after Western blotting.

Protein–protein docking

The crystal structure files of MYO6 and its target proteins were downloaded from the Protein Data Bank (PDB) database (https://www.rcsb.org/). Before docking, PDB files were prepared as follows: hydrogen molecules were added, extraneous water molecules were removed, and pH-sensitive protonation was adjusted using SYBYL-X 2.0 software. Protein–protein docking was conducted through the docking program HEX 8.0.0 software. The MYO6 protein–FAK–FREM complex analysis was performed via the ZDOCK server.

In vivo tumorigenesis assay

Male BALB/c nude mice (6–7 weeks old) were obtained from the animal medical center affiliated with the Shanghai cancer center of Fudan University. 22Rv1-shCN or 22Rv1-shMYO6 (5×10^6 cells) premixed with Matrigel (Corning) at a 1: 1 ratio was injected subcutaneously into the upper flank region of the mice. When the tumor volume reached 50 mm^3, the mice were randomly divided into four groups ($n=6$ for each group) and treated with Enz (30 mg/kg), the FAK inhibitor Y15 (5 mg/kg), Enz (30 mg/kg)+Y15 (5 mg/kg) or the control solvent every other day for 3 weeks. The tumor size and volume were measured every two days. On the third day after the last dosing, the mice were euthanised and the tumors were dissected for further analysis. The animal experiment protocols used were approved by the Institutional Animal Care and Use Committee of Shanghai Veterinary Research Institute (SV-20220916-03).

Gene expression omnibus (GEO) and cBioPortal databases

The public GEO database (https://www.ncbi.nlm.nih.gov/geo), which allows researchers to share data for common analysis, and another comprehensive database, cBioPortal (http://www.cbioportal.org), which contains data from different databases, such as The Cancer Genome Atlas database (TCGA), were used in this study. The data were analyzed with R software (version 4.1.1).

Statistical analysis

The data were collected from at least three independent experiments except where specified and are expressed as the means±standard deviations (SDs). Categorical variables are presented as numbers or percentages. The samples were randomly allocated to different treatment conditions. Representative areas of the cell culture chambers were randomly selected for imaging with a microscope. All testing and data analysis were conducted in a blinded manner. The statistical methods used included Student's *t*-test, ANOVA, the χ^2 test, Spearman's correlation analysis, the Mann–Whitney U test (for non-normally distributed data between two groups), and receiver operating characteristic analysis (ROC) for diagnostic efficiency. Survival curves were constructed using Kaplan–Meier survival analysis and compared using the log-rank test. All the statistical analyses were performed using SPSS software (version 21.0). $P<0.05$ was considered to indicate statistical significance.

Results

MYO6 expression is upregulated in PCa tissues and Enz-resistant cells and is associated with adverse clinical features

We investigated the level of MYO6 expression in PCa tissues and adjacent normal prostate tissues from our center (Fudan University Shanghai Cancer Center, FUSCC) and found that the protein expression level and IHC score of MYO6 in PCa tissues was greater than those in adjacent normal prostate tissues (Fig. 1A–C). To verify the MYO6 expression in PCa tissues, we analyzed high-throughput data from the TCGA database and found that the MYO6 mRNA level in PCa tissues was significantly greater than that in normal prostate tissues (Fig. 1D). In addition, the MYO6 mRNA expression level obviously increased in patients with higher Gleason scores (Fig. 1E). Furthermore, MYO6 mRNA expression levels were greater in PCa tissues than in normal tissues according to the GSE6919 and GSE70768 datasets from the GEO database (Fig. 1F, G). The clinical feature analysis of GSE70768 dataset showed a shorter time to

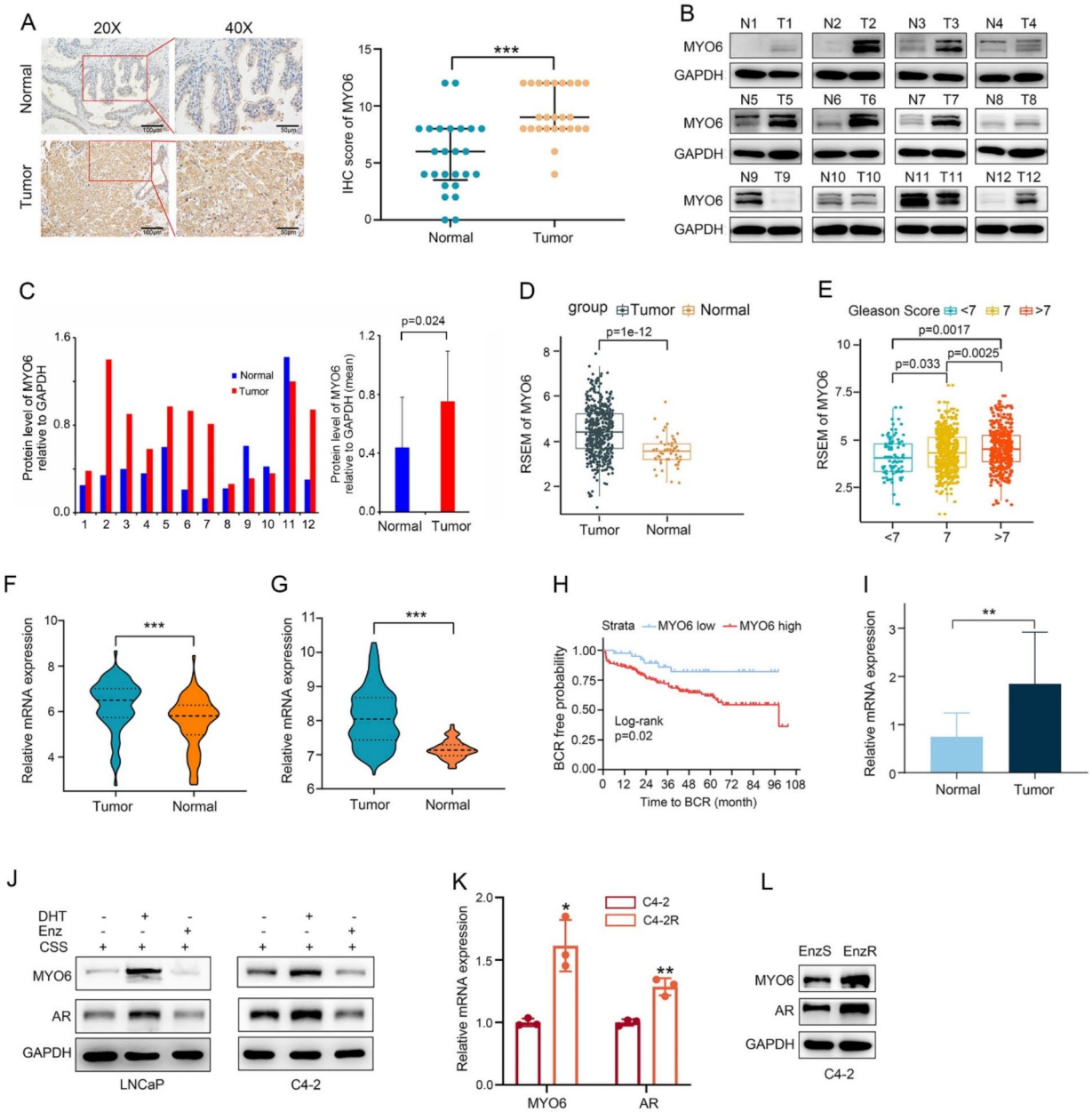

Fig. 1 MYO6 expression is correlated with PCa and the development of Enz resistance. **A** Representative images of MYO6 stained using IHC in PCa tissues and adjacent normal prostate tissues, and the MYO6 expression was shown as an IHC score (Mann–Whitney U test). **B**–**C** Experimental analysis of the MYO6 expression level in the FUSCC cohort. The protein expression of MYO6 in PCa tissues and normal prostate tissues were determined using immunoblotting, and the relative protein level was estimated by image J software ($n = 12$). **D**–**H** Statistical analysis of MYO6 expression in the public dataset. The expression of MYO6 in PCa tissues and normal prostate tissues was analyzed based on the TCGA (tumor, $n = 500$; normal, $n = 51$) dataset (D) and different Gleason score samples from the TCGA (E). The mRNA expression of MYO6 in PCa tissues and normal prostate tissues from the GSE6919 dataset (tumor, $n = 90$; normal, $n = 81$) (F) and GSE70768 dataset (tumor, $n = 206$; normal, $n = 74$) (G). Kaplan-Meier plots revealing different probabilities of biochemical recurrence (BCR)- free survival after radical prostatectomy in patients with low MYO6 expression ($n = 43$) and high MYO6 expression ($n = 157$) in the GSE70768 cohort (H). **I** The mRNA expression of MYO6 in PCa tissues ($n = 25$) and adjacent normal prostate tissues ($n = 25$) detected by RT–qPCR. **J** Western blotting analysis of MYO6 and AR expression in LNCaP and C4-2 cells cultured in charcoal-stripped serum (CSS) medium and treated with DHT (2 nM) or Enz (10 μM) for 48 h. **K–L** The mRNA and protein expression levels of MYO6 and AR in Enz-sensitive (EnzS)-C4-2 and Enz-resistant (EnzR)-C4-2 cell lines were detected by RT–qPCR and Western blotting, respectively. Data were expressed as the mean ± SD. $^{*}p < 0.05$, $^{**}p < 0.01$, $^{***}p < 0.001$

biochemical relapse (BCR) in patients with high MYO6 expression than that in patients with low MYO6 level (Fig. 1H). Additionally, the mRNA expression of MYO6 was determined in PCa tissues using RT-qPCR, and the result showed that MYO6 significantly increased in PCa (Fig. 1I), which was consistent with the results from the GEO and TCGA data. Moreover, a high MYO6 expression level was associated with tumor T stage and was also observed in the nonsurviving group than in the surviving group (Table 1). We suggest that the survival of patients with localized PCa who underwent radical surgery has a good prognostic value. As a result, we did not observe significant difference in MYO6 expression in survival analysis. There were also no obvious differences in MYO6 expression according to age, race, or N/M stage (Table 1). Notably, analysis of the pancancer data showed that MYO6 expression was significantly increased in PCa and breast cancer tissues compared to other cancer tissue samples, indicating that MYO6 is likely a hormone-regulatory gene (Fig. S1A). Additionally, MYO6 expression was significantly enhanced by DHT and decreased by Enz in charcoal-stripped serum (CSS)-starved LNCaP cells, as well as in C4-2 cells (Fig. 1J). Finally, the Enz-resistant cell line C4-2R was successfully constructed with the IC50 of 43.05 μM (for C4-2 cell lines, the IC50 = 12.25 μM; for LNCaP cell lines, the IC50 = 8.70 μM) (Fig. S1B, C). The upregulation of MYO6 and AR expression was simultaneously observed in the Enz-resistant cell line C4-2R compared with the Enz-sensitive cell line C4-2 (Fig. 1K, L). No significant variants of AR and MYO6 were observed in C4-2R treated with Enz (Fig. S1D). These data indicate that high expression of MYO6 may be correlated with PCa and Enz resistance.

MYO6 promotes PCa cell progression by targeting BCL-2/caspase-3 and the EMT

Previous studies have revealed that MYO6 inhibition suppressed the growth of the PCa cell lines DU145 and PC-3 [17]. To comprehensively examine the effect of MYO6 expression on the proliferation, invasion, and migration of PCa cells, LNCaP, C4-2, and 22Rv1 cells were used to construct stable cell lines with MYO6 knockdown or overexpression. The efficiency of MYO6 knockdown or overexpression was verified using RT−qPCR and Western blotting (Fig. 2A–D). Using these cell lines, we validated the role of MYO6 expression in PCa cells and revealed that MYO6 silencing decreased cell viability, clonogenicity, invasion, and migration in LNCaP, C4-2, and 22Rv1 cells (Fig. 2E–G and K–M and Fig. S2A, G, 3 A–C, 3G–I). In contrast, MYO6 overexpression enhanced these cell phenotypes in LNCaP, C4-2, and 22Rv1 cells (Fig. 2H–J and Fig. S2B, H, 3D–F, 3 J–L).

To further investigate the role of MYO6 in regulating the proliferation of PCa cells, we performed flow cytometry assays. Cell cycle analysis revealed that the percentage of LNCaP and C4-2 cells in S phase significantly decreased when MYO6 expression was suppressed, indicating that MYO6 plays an important role in G0/G1 stage

Table 1 Correlation between MYO6 expression and clinicopathological features in PCa patients from the TCGA dataset ($n = 551$, mean ± SD)

Clinical characteristics	Case (*n*)	MYO6 expression level	*p* value
Sample			
Tumor	500	4.45 ± 1.07	$p < 0.05$
adjacent	51	3.57 ± 0.66	
Age at diagnosis (years old)			
≤ 65	333	4.45 ± 1.08	$p = 0.94$
> 65	167	4.44 ± 0.05	
Survival			
Yes	488	4.43 ± 1.06	$p = 0.05$
No	10	5.09 ± 1.07	
Unknown	2		
T stage			
T1 ~ 2	188	4.31 ± 1.10	$p < 0.05$
T3 ~ 4	305	4.54 ± 1.04	
Unknown	7		
N stage			
N0	348	4.43 ± 1.08	$p = 0.09$
N1	79	4.66 ± 1.04	
Unknown	73		
Race			
White	415	4.45 ± 1.05	$p = 0.24$
African American/Asian	71	4.61 ± 1.12	

MYO6, myosin VI; PCa, prostate cancer; TCGA, The Cancer Genome Atlas; SD, standard deviation. Statistical analysis was performed by two-sided Student's *t*-test

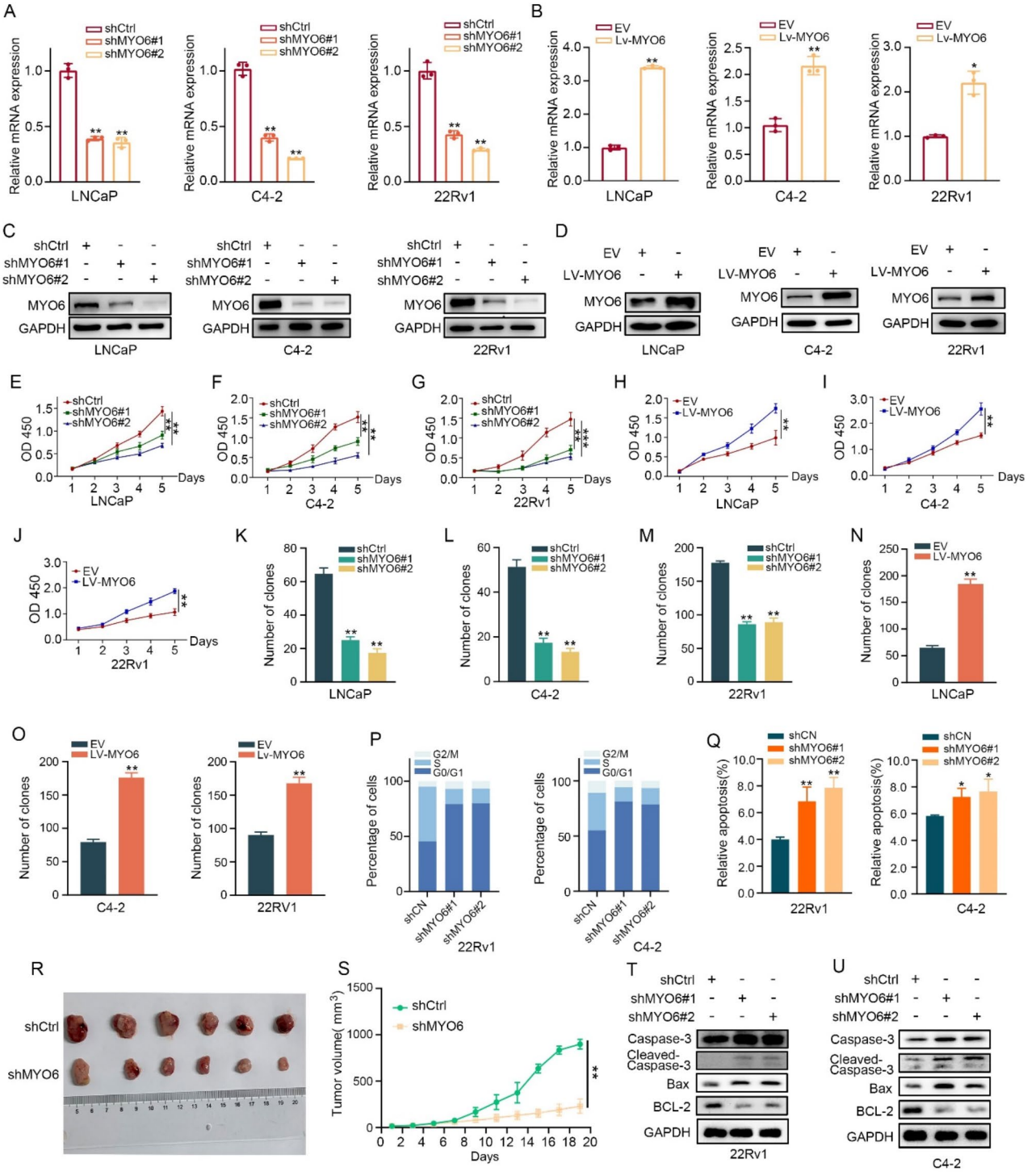

Fig. 2 MYO6 promotes PCa cell proliferation and tumorigenesis in vitro and in vivo. **A**–**D** Lentiviral plasmids carrying MYO6 or MYO6-targeting shRNA were used to construct the corresponding cell lines, and RT–qPCR and Western blotting were subsequently conducted to evaluate MYO expression at the mRNA and protein expression levels, respectively. **E**–**G** The proliferation of LNCaP, C4-2, and 22Rv1 cells lines transfected with shCtrl or shMYO6 was assessed through a CCK-8 assay. **H**–**J** The proliferation of LNCaP, C4-2, and 22Rv1 cells lines transfected with EV or LV-MYO6 was assessed through a CCK-8 assay. **K**–**M** The colony numbers of LNCAP, C4-2, and 22Rv1 cells lines transfected with shCtrl or shMYO6 were evaluated through a colony formation assay. **N**–**O** The colony numbers of LNCAP, C4-2, and 22Rv1 cells lines transfected with EV or LV-MYO6 were evaluated through a colony formation assay. **P**–**Q** Cell cycle distribution (P) and cell apoptosis (Q) in LNCaP and C4-2 cells lines transfected with shCN or shMYO6 were analyzed through flow cytometry assays. **R**–**S** Tumorigenesis analysis of 22Rv1 cell lines transfected with shCtrl or shMYO6 in mice. **T**–**U** The protein expression levels of Cleaved caspase-3/caspase-3 and Bax/BCL-2 in 22Rv1 and C4-2 cells lines transfected with shCtrl or shMYO6 were determined via Western blotting, which indicates that MYO6 depression increases the caspase-3 protein expression and decreases the BCL-2 protein expression. *$p < 0.05$, **$p < 0.01$, ***$p < 0.001$

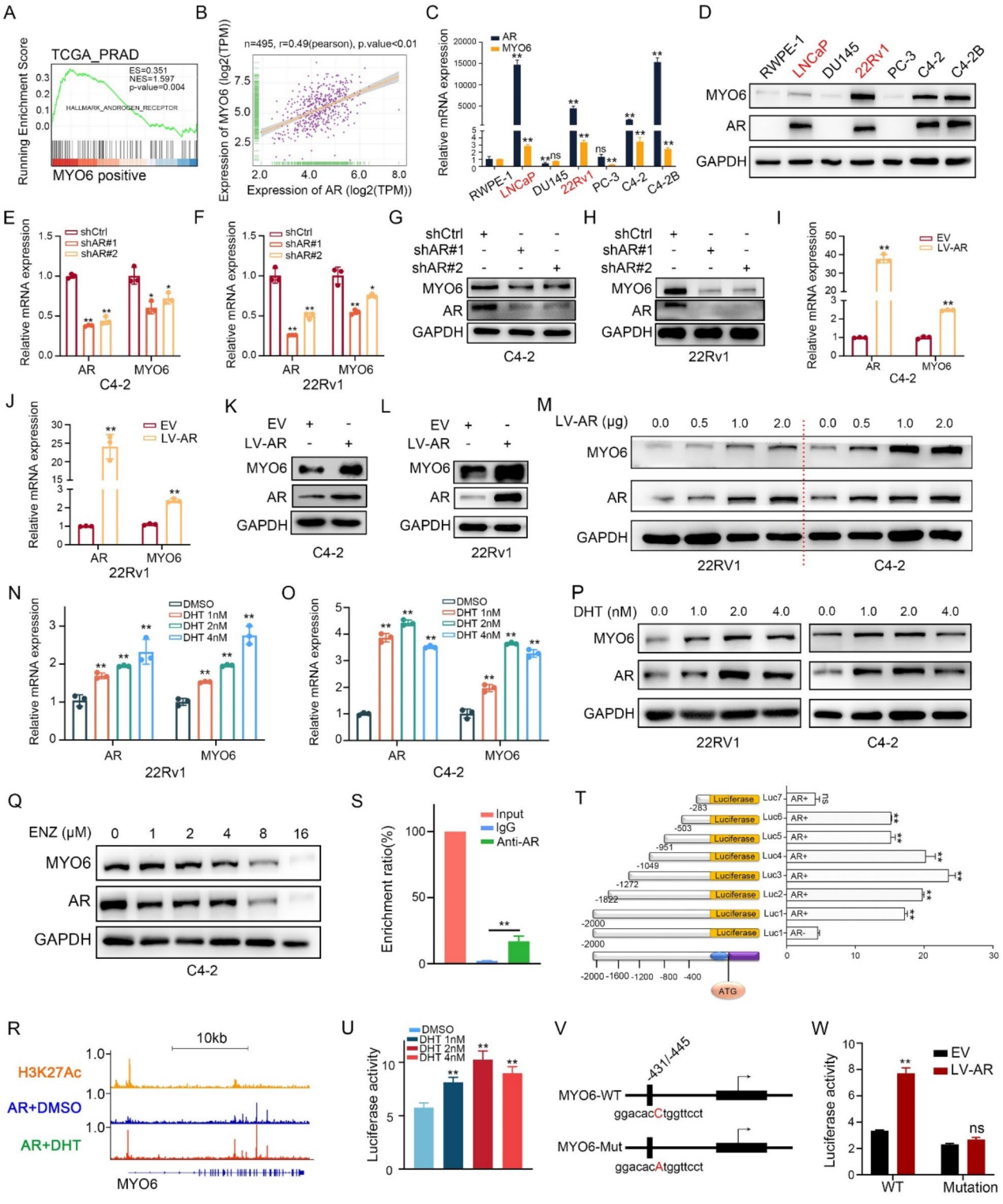

Fig. 3 (See legend on next page.)

(See figure on previous page.)

Fig. 3 Identification of AR as an upstream regulator of MYO6. **A** GSEA of the effect of MYO6 expression on androgen response signaling. **B** Pearson's correlation analysis of the relationship between MYO6 and AR expression. **C**–**D** The mRNA and protein expression levels of MYO6 and AR in PCa cell lines were detected by RT–qPCR and Western blotting, respectively. **E**–**H** The mRNA and protein expression levels of MYO6 and AR in the C4-2 and 22Rv1 cell lines transfected with shCtrl or shAR were detected by RT–qPCR and Western blotting, respectively. **I**–**L** The mRNA and protein expression levels of MYO6 and AR in the C4-2 and 22Rv1 cell lines transfected with EV or LV-AR were detected by RT–qPCR and Western blotting, respectively. **M** The effect of different doses of AR on the protein expression of MYO6 and AR in the 22Rv1 and C4-2 cell lines was determined by Western blotting. **N**–**P** The effects of different concentrations of DHT on the mRNA and protein expression of AR and MYO6 in the 22Rv1 and C4-2 cell lines were determined by RT–qPCR and Western blotting, respectively. **Q** The effects of different concentrations of Enz on the protein expression of MYO6 and AR in C4-2 cells lines were determined by Western blotting. **S** ChIP–qPCR analysis of AR binding to the *MYO6* promoter in LNCaP cell lines. **T** Dual-luciferase dissection of the AR response element in the *MYO6* promoter (residues − 503 bp to − 283 bp). **R** The extent to which AR binds to the *MYO6* promoter was analyzed via ChIP-seq analysis. **U** The effect of different concentrations of DHT on the luciferase activity of PCa cell lines. (**V**) A mutant luciferase reporter plasmid with a MYO6 promoter sequence containing a point mutation at the AR binding site. **W** Luciferase activity in WT or mutant PCa cell lines treated with EV or LV-MYO6. ns, nonsignificant; *$p < 0.05$, **$p < 0.01$

cell arrest (Fig. 2P and Fig. S2C–D). Cell apoptosis analysis also revealed that MYO6 inhibition increased the apoptosis rate of LNCaP and C4-2 cells (Fig. 2Q and Fig. S2E–F). Based on the evidence above, the progression of PCa promoted by MYO6 primarily occurs through the regulation of the cell cycle, while its influence on apoptosis is weaker. In addition, the tumor growth of 22Rv1 cells was attenuated when MYO6 expression was suppressed in vivo (Fig. 2R–S).

The epithelial–mesenchymal transition (EMT) is an essential process in the transition of cancer cells to advanced metastatic status [23]. We investigated the role of MYO6 expression in EMT, and the results indicated that the protein expression level of E-cadherin was upregulated, whereas the expression of snail 1, N-cadherin, and vimentin was suppressed when MYO6 expression was knocked down (Fig. S3M–N). Accordingly, MYO6 overexpression decreased E-cadherin expression (Fig. S3O). These results suggest that MYO6 might enhance the metastasis of PCa by promoting the EMT process. As previous studies reported that the caspase-3/BCL-2 axis plays an important role in PCa cell proliferation [24, 25], we then analyzed the molecular mechanism by which MYO6 regulates PCa cell proliferation, and the results indicated that the ratio of Cleaved-caspase-3/procasepase-3 and Bax/BCL-2 was increased after MYO6 suppression (Fig. 2T–U). Collectively, these data indicate that MYO6 promotes PCa progression through multiple pathways and that the malignant phenotype of PCa occurs mainly through targeting the BCL-2/caspase-3 axis and the EMT.

Identification of AR as an upstream regulator of MYO6

As MYO6 expression increases in Enz-resistant PCa cells and AR plays a critical role in this process, the RNA-seq profile from the TCGA database was used to analyze the relationship between MYO6 and AR. The GSEA results indicated that MYO6 promoted the expression of androgen response signals (Fig. 3A). Pearson's correlation analysis revealed that MYO6 was positively coexpressed with AR (Fig. 3B). Next, we detected the mRNA and protein expression levels of MYO6 in AR-negative and AR-positive PCa cell lines, and the results showed that both the mRNA and protein expression levels of MYO6 in AR-positive cells were greater than those in AR-negative cells (Fig. 3C–D). We further showed that MYO6 expression was attenuated at both the mRNA and protein expression levels when AR expression was knocked down in several AR-positive PCa cell lines (Fig. 3E–H). Conversely, AR overexpression increased the expression of MYO6 in 22Rv1 and C4-2 cells (Fig. 3I–L). Moreover, the protein expression level of MYO6 increased in a dose-dependent manner with AR accumulation (Fig. 3M), and DHT treatment increased AR expression and promoted MYO6 transcription (Fig. 3N–P and Fig. S4F–G). Conversely, Enz treatment decreased the protein expression of MYO6 in the Enz sensitive cell lines (Fig. 3Q). As expected, activation of AR by DHT or overexpression of AR increased the expression of KLK3, a well-known AR target gene in both 22Rv1 and C4-2 cells (Fig. S4C-E).

On the basis of these data, we hypothesized that MYO6 is transcriptionally regulated by AR. To verify this hypothesis, we checked the ChIP-seq data and found strong binding of AR to the promoter region of *MYO6*, and this binding was robustly stronger in response to DHT stimulation (Fig. 3R). Furthermore, we conducted ChIP−qPCR assay to confirm that the transcription factor AR was recruited to the promoter region of *MYO6* (Fig. 3S). To uncover the potential molecular mechanism by which AR regulates MYO6 in AR-positive PCa cells, we cloned a series of MYO6 promoter truncation mutants into vectors with luciferase reporter genes (Luc1 to Luc7) (Fig. 3T) and found that AR overexpression enhanced the MYO6-related luciferase activity of Luc1, Luc2, Luc3, Luc4, Luc5, and Luc6 constructs but not Luc7, indicating that the minimum AR binding site in the *MYO6* promoter is within the −503 to −283 bp (bp) region. The luciferase activity was also enhanced by DHT treatment (Fig. 3U). In addition, a mutant luciferase reporter plasmid with a *MYO6*-point mutation in the promoter sequence (GGACAC**c**TGGTTCCT → GGACAC**a**TGGTTCCT) at the AR binding site (residues −503 bp to −283 bp) was termed *MYO6*-mutuant (Mut) (Fig. 3V), and the reporter system containing a wild-type

(WT) *MYO6* promoter within the AR binding site was used as the control (MYO6-WT). The results showed that AR overexpression increased MYO6 luciferase activity in MYO6-WT reporter system cells and that this effect was attenuated when the AR binding site was mutated in C4-2 cells (Fig. 3W). Taken together, these data suggest that AR positively regulates MYO6 expression and that this regulation occurs at the transcriptional level.

Targeting MYO6 suppresses focal adhesion signals to overcome Enz resistance

Enz is a potent next-generation AR signaling inhibitor that is a first-line drug for CRPC treatment. Unfortunately, CRPC frequently progresses to Enz-resistant CRPC, indicating a poor prognosis [26] after a median of 18 months of treatment. Here, we constructed the Enz-resistant CRPC cell C4-2R by stimulating the CRPC cell C4-2 with Enz (as described in the Materials and methods section).

Based on the key role of MYO6 in Enz resistance, we performed RNA-seq analysis between C4-2 and C4-2R to determine differentially expressed genes (DEGs) related to Enz resistance (Fig. 4A) and to determine the DEGs associated with MYO6 silencing in C4-2R cells (Fig. 4B). After screening, a total of 137 gene signatures were considered to be Enz resistance response genes and also candidate genes regulated by MYO6 (Fig. 4C–E). Following Gene Ontology (GO) and Kyoto Encyclopedia of Genes and Genomes (KEGG) analyses, we observed that downstream genes related to MYO6 signaling were involved in multiple cellular biological processes, including cell junction assembly and synapse organization (biological processes), glutamatergic synapse, postsynaptic specialization, neuron to neuron synapse (cell components), and transmembrane receptor protein kinase activity and collagen binding (molecular function) (Fig. 4F, G). According to the KEGG analysis, the target genes were involved in mainly focal adhesion, gap junctions, the cAMP signaling pathway, and the calcium signaling pathway (Fig. 4G).

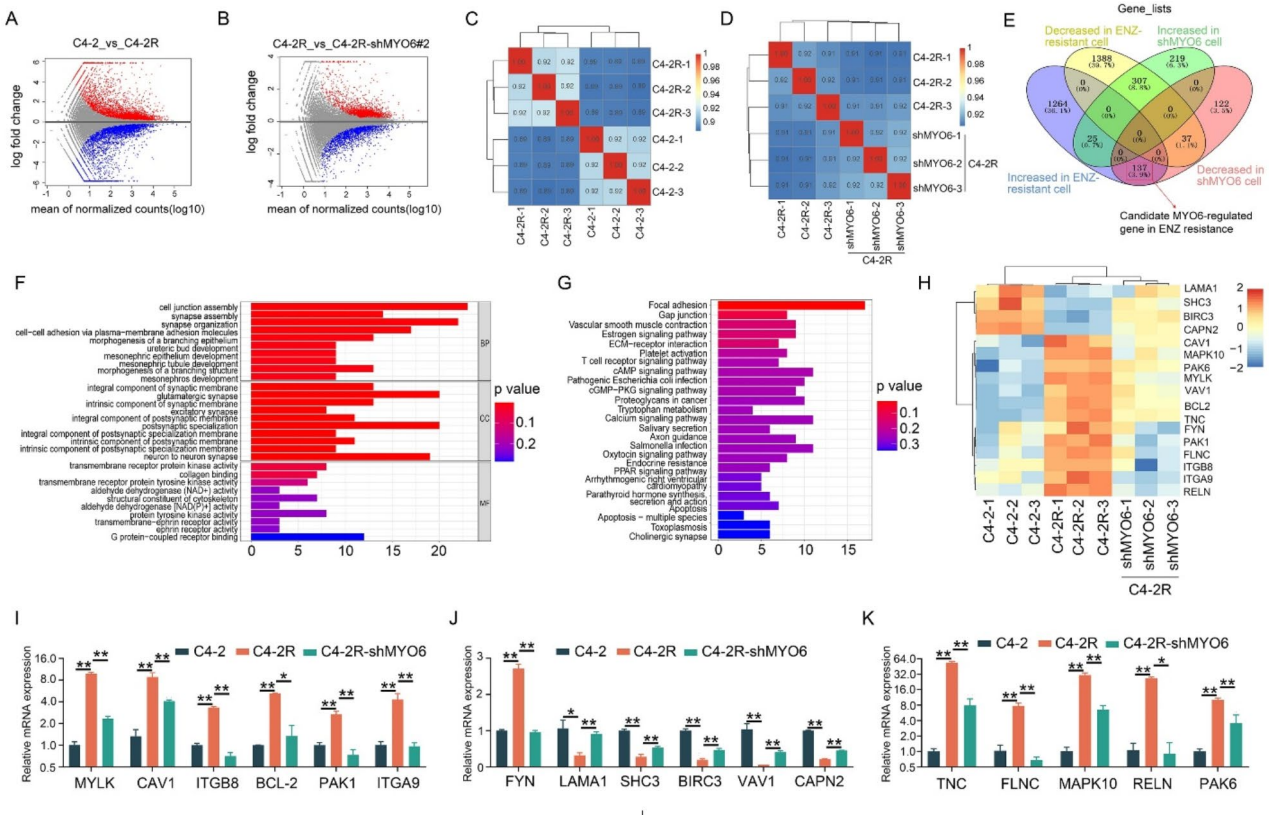

Fig. 4 RNA-seq reveals MYO6-associated gene sets involved in the development of Enz resistance. **A**–**B** MA plots of DEGs between the C4-2 and C4-2R cell lines (A) and of the MYO6 response genes between the C4-2R cell lines transfected with or without shMYO6 (B) were generated by RNA-seq analysis. **C**–**D** Pearson's correlation analysis of the correlation between the C4-2R and C4-2 cell lines (C) and between the C4-2R and C4-2R cell lines transfected with shMYO6 (D). **E** Venn diagram analysis of a total of 137 MYO6-regulated genes during the development of Enz resistance. **F** Gene Ontology analysis of the involvement of MYO6 in biological processes such as cell junction assembly and synaptic organization. **G** KEGG analysis of the MYO6-regulated genes, which were enriched mainly in the focal adhesion pathway. **H** Heatmap of the MYO6-regulated genes in the focal adhesion pathway in the C4-2, C4-2R, and C4-2R cell lines transfected with shMYO6. **I**–**K** The mRNA expression of the genes enriched in the focal adhesion pathway in the C4-2, C4-2R, and C4-2R shMYO6 cell lines was detected via RT–qPCR, which was consistent with the results of the RNA-seq analysis. *$p < 0.05$, **$p < 0.01$

Taken together, these enrichment results suggested that MYO6 may act mainly as a regulator of the focal adhesion signaling, maintaining cell growth and Enz resistance. To this end, the mRNA expression levels of genes enriched in the focal adhesion pathway in C4-2R and C4-2R-shMYO6 cells are shown in Fig. 4H, which shows that the genes enriched in the focal adhesion pathway were more highly expressed in C4-2R cells. Notably, the expression of these genes was reversed in C4-2R cells when MYO6 was knocked down, indicating that these genes participate in Enz resistance and are regulated by MYO6. These results were also verified by RT−qPCR (Fig. 4I–K). However, the mRNA and protein expression levels of FAK, a key protein in the focal adhesion signal transduction pathway, did not change significantly during this process; it is unknown whether this indicates that FAK activity is affected by post-translation modification (PTM).

Recently, studies have reported that phosphorylation at the Y397 residue in FAK plays an essential role in FAK function [27]. First, no significant difference in FAK mRNA expression was observed between the Enz-resistant cells and MYO6-knockdown cells (Fig. 5A–B) or MYO6 overexpression cells (Fig. 5C). However, the phosphorylation level of the FAK protein at Y397 was downregulated when MYO6 expression was knocked down in the Enz-resistant cells (Fig. 5D–F), whereas MYO6 overexpression enhanced the phosphorylation level of the Y397 residue in FAK (Fig. 5G). Notably, previous studies have suggested that integrin subunit beta 8 (ITGB8) regulates FAK activity through the upregulation of FAK protein expression [28]. Interestingly, in this study we observed that ITGB8 expression increased in C4-2R cells compared to C4-2 cells, whereas ITGB8 expression decreased in C4-2R-shMYO6 cells compared to C4-2R cells, indicating that MYO6 promoted FAK phosphorylation at residue Y397 to activate focal adhesion signaling by ITGB8 modulation (Fig. 5D–G). The phosphorylation level of Y397-FAK was decreased after knocking down ITGB8, whereas the phosphorylation level of Y397-FAK was increased when overexpressing ITGB8 in C4-2 cells (Fig. 5H–I). Additionally, ITGB8 overexpression could restore the phosphorylation level of Y397-FAK that was inhibited by MYO6 suppression (Fig. 5I–J). The interaction between ITGB8 and FAK was also observed, which was consistent with previous reports (Fig. 5K). However, there is little evidence to explain the way ITGB8 interacts with FAK and promotes FAK phosphorylation. Our molecular docking results revealed that ITGB8 binds well to FAK (Etotal: -1391.44) through the integrin domain but not the EGF-like domain (Fig. 5L–M). Furthermore, we found that the main interacting amino acids were glutamic acid on ITGB8 and arginine on FAK (Fig. 5M; wheat color indicates the FAK protein, and blue color indicates the ITGB8 protein). Consistently, GST pull-down analysis also revealed that the integrin domain interacted with FAK (Fig. 5N–O). The interaction between ITGB8 and FAK was modulated when altering glutamate on the integrin domain of ITGB8 with arginine (Fig. 5P). Furthermore, the pFAK (Y397-FAK) level was decreased by Enz treatment within 48 h, but the pFAK level increased after 6 or more days of continuous treatment (Fig. 5Q).

A previous study demonstrated that suppressing the phosphorylation of pFAK at the Y397 residue inhibited the expression and secretion of vascular endothelial growth factor A (VEGFA), which consequently repressed angiogenesis [27]. Our data showed that VEGFA protein expression was downregulated when MYO6 was silenced and VEGFA protein expression was upregulated when MYO6 was overexpressed (Fig. 5D–G). Y15 has been reported to be an inhibitor of the crystal structure of FAK [29, 30]. We verified its function and found that Y15 specifically inhibited the pY397-FAK level in PCa cells (Fig. S5A–B), which was used as an efficient agent to inhibit the function of FAK in this study. Collectively, these data suggest that FAK is a downstream target of the AR/MYO6 axis and is closely related to Enz resistance.

FAK inhibition enhances the sensitivity of PCa cells to Enz

To determine the key role of MYO6 overexpression in the development of Enz resistance in CRPC cells, we treated Enz-resistant cells with Enz and found that the IC50 of Enz decreased from 32.75 μM to 7.27 μM in 22Rv1 cells and from 41.97 μM to 14.23 μM in C4-2R cells with MYO6 knockdown (Fig. 6A–B and Fig. S4A–B). To test the role of MYO6 in Enz resistance, we constructed stable MYO6-knockdown cell models in four different PCa cell lines. CCK-8 assay results revealed that the average percentages of MYO6-knockdown cells inhibited by Enz treatment (LNCaP-shMYO6#2: 43.6%, 22Rv1-shMYO6#2: 40.0%, C4-2-shMYO6#2: 45.0%, and C4-2R-shMYO6#2: 44.9%) were significantly higher than those of the control cells (LNCaP-shCtrl: 30.0%, 22Rv1-shCtrl: 5.0%, C4-2-shCtrl: 30.5%, and C4-2R-shCtrl: 13.9%) on day 5 (Fig. 6C–J). Interestingly, suppressing the FAK expression via shRNA significantly inhibited the proliferation of 22Rv1 and C4-2R cells (Fig. 6K–N); notably, 22Rv1 and C4-2R cells also exhibited restored sensitivity to Enz treatment (Fig. 6O–P). We also investigated the inhibitory effect of Y15 on 22Rv1 and C4-2R cells, and the results showed that the IC50 of Enz decreased in 22Rv1 and C4-2R cells when Enz treatment was administered in combination with Y15 (Fig. 6Q–R). Furthermore, the combination treatment of Enz and Y15 had the strongest inhibitory effect on the proliferation of Enz-resistant cells compared with that of Enz or Y15 alone (Fig. 6S–U), suggesting that targeting FAK with Y15 may be an ideal

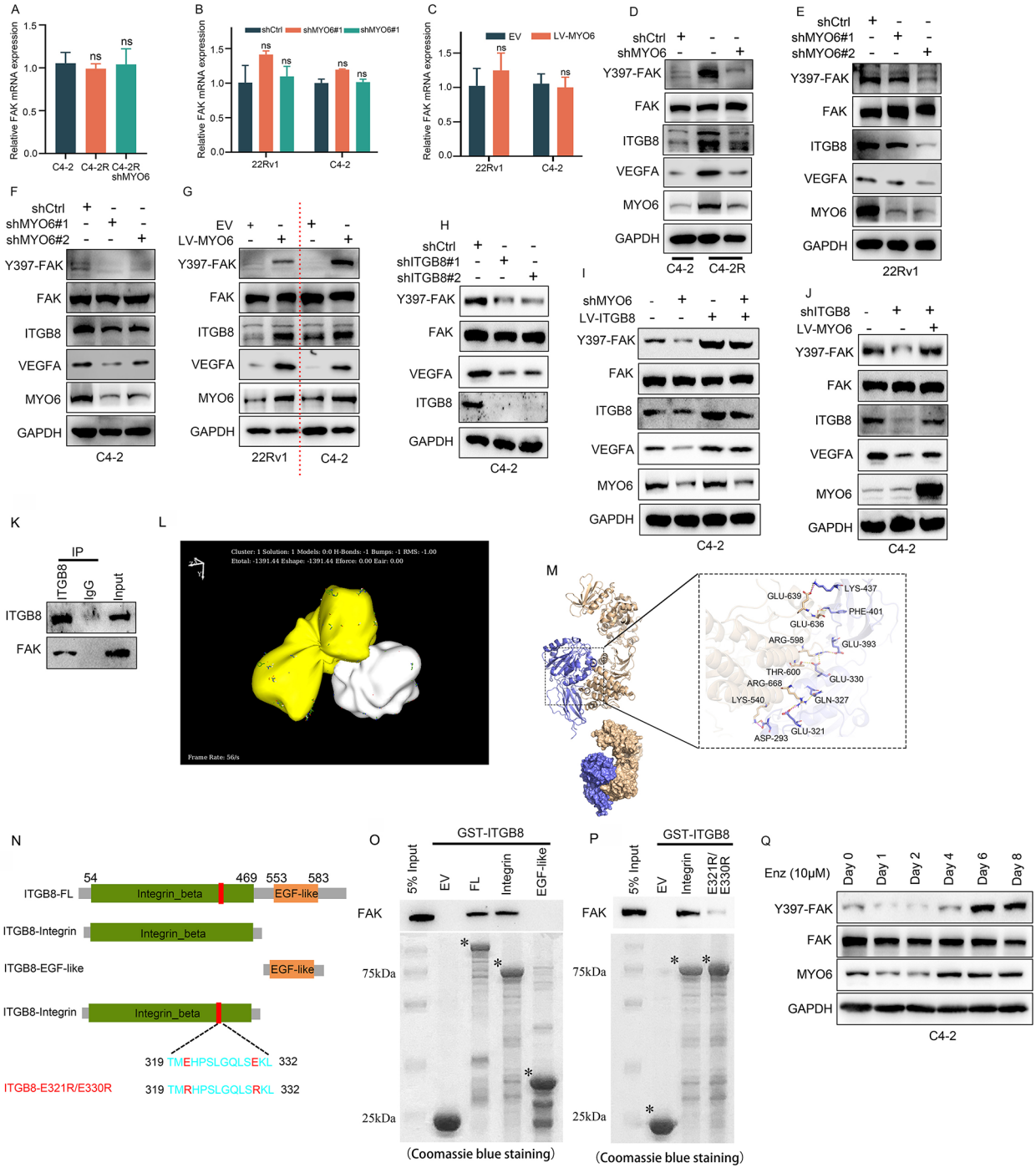

Fig. 5 MYO6 activates the focal adhesion pathway by promoting phosphorylation of the key protein FAK. **A**–**C** The mRNA expression of FAK in the C4-2 and C4-2R cell lines transfected with or without shMYO6 (A), the 22Rv1 and C4-2 cell lines transfected with shCtrl or shMYO6 (B), and the 22Rv1 and C4-2 cell lines transfected with EV or LV-MYO6 (C) was detected by RT–qPCR. **D**–**F** The protein levels of pY397-FAK, FAK, ITGB8, VEGFA, and MYO6 in C4-2 and C4-2R cells transfected with shCtrl or shMYO6 (D) and 22Rv1 and C4-2 cells transfected with shCtrl or shMYO6 (E, F) were detected via Western blotting. **G** The protein levels of pY397-FAK, FAK, ITGB8, VEGFA, and MYO6 in 22Rv1 and C4-2 cells transfected with EV or LV-MYO6 were detected via Western blotting. **H** The protein levels of pY397-FAK, FAK, VEGFA, and ITGB8 in C4-2 cells transfected with shCtrl or shITGB8 were detected via Western blotting. **I**–**J** The protein levels of pY397-FAK, FAK, ITGB8, VEGFA, and MYO6 in C4-2 cells transfected with shMYO6 or LV- ITGB8 (I) and shITGB8 or LV-MYO6 (J) were detected via Western blotting. **K** Interaction between ITGB8 and FAK was analyzed via immunoprecipitation assays. **L** The protein–protein docking interaction between MYO6 and FAK was analyzed with HEX software (white color indicates the MYO6 protein, and yellow color indicates the FAK or FREM domain). **M** The main interacting amino acids were glutamic acid on ITGB8 and arginine on FAK (wheat color indicates the FAK protein, and blue color indicates the ITGB8 protein). **N**–P GST-pull-down analysis of the ITGB8 integrin domain interacted with FAK (N) and the interaction between ITGB8 and FAK (O, P). **Q** The protein levels of pY397-FAK and FAK in C4-2 cells treated with Enz were detected via Western blotting. ns, nonsignificant; $^{*}p < 0.05$

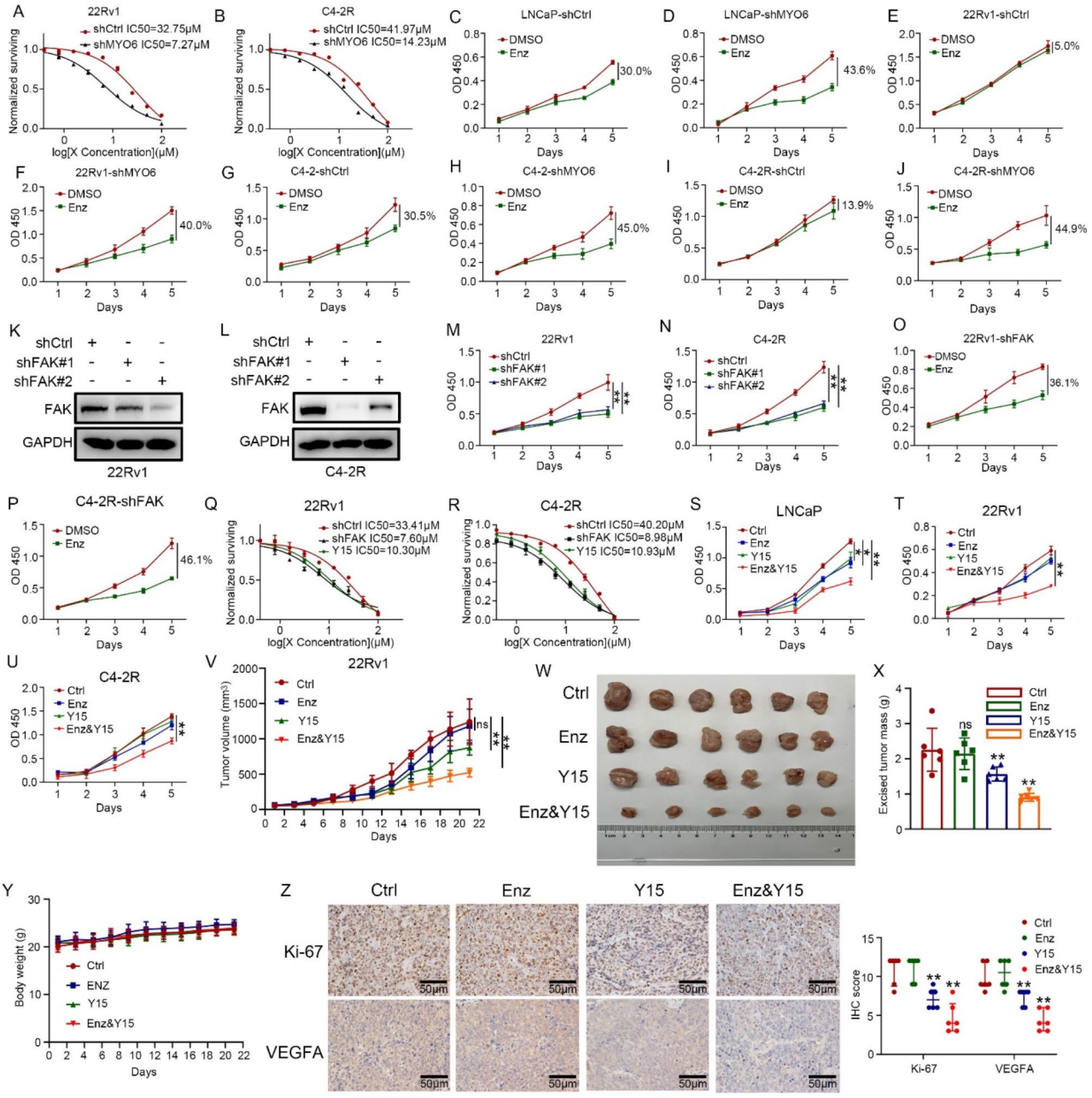

Fig. 6 Targeting MYO6 resensitizes EnzR cells to Enz and suppresses EnzR cell growth in vitro and in vivo. **A**–**B** The IC50s of Enz in the 22Rv1 and C4-2R cell lines transfected with shCtrl or shMYO6 for 22Rv1 (from 32.75 to 7.27 μM) and for C4-2R (from 41.97 to 14.23 μM). **C**–**J** The viability of LNCaP, 22Rv1, C4-2, and C4-2R cells transfected with shCtrl or shMYO6 and treated with Enz (5 μM for LNCaP and C4-2 cells; 20 μM for 22Rv1 and C4-2R cells) was evaluated through a CCK-8 assay. **K**–**L** The protein expression of FAK in the 22Rv1 and C4-2R cell lines transfected with shCtrl or shFAK was detected by Western blotting. **M**–**N** The proliferation of 22Rv1 and C4-2R cells treated with shCtrl or shFAK was assessed through a CCK-8 assay. **O**–**P** The proliferation of 22Rv1 and C4-2R cells treated with shFAK and Enz was assessed through a CCK-8 assay. **Q**–**R** Comparison of the IC50s of Enz in 22Rv1 and C4-2R cells treated with shCtrl or shFAK and administered Y15 treatment. **S**–**U** The viability of LNCaP, 22Rv1, and C4-2R cells treated with Enz, Y15, or Enz+Y15 was evaluated through a CCK-8 assay. **V–Y**The proliferation of 22Rv1 cells in mice treated with Enz, Y15, or Enz+Y15. Tumor growth curves were constructed (V), tumors were collected and photographed (W), and tumor weights (X) and mouse body weights (Y) were measured ($n=6$ mice/group). **Z** IHC staining of Ki-67 and VEGFA in tumor xenografts from (W) was conducted, and staining scores were quantified and compared. ns, nonsignificant; $^{*}p<0.05$, $^{**}p<0.01$, $^{***}p<0.001$

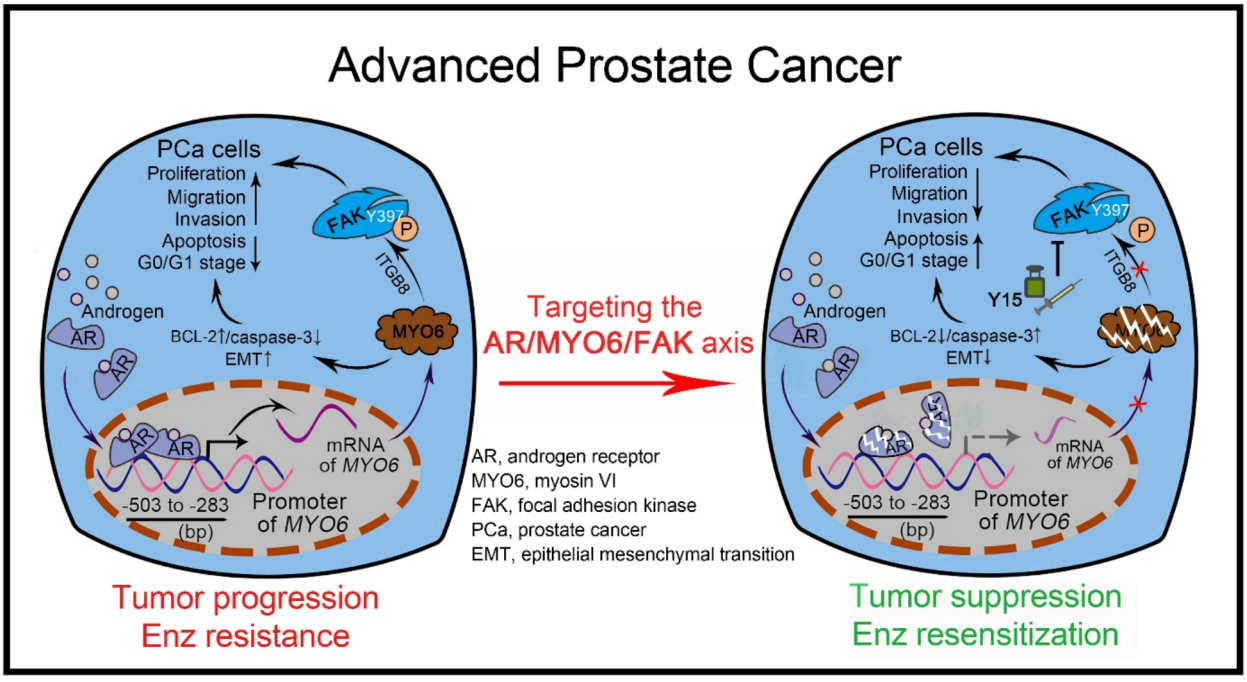

Fig. 7 Proposed mechanistic scheme of AR/MYO6/FAK axis in CRPC (advanced prostate cancer). This study showed that AR transcriptionally upregulates MYO6 expression via directly binding to the MYO promoter to enhance the FAK phosphorylation, which promotes PCa progression and Enz resistance. Targeting the AR/MYO6/FAK axis inhibits PCa progression and resensitizes CRPC cells to Enz treatment. Y15, an inhibitor of FAK, is strongly effective in inhibition of tumor growth in PCa by inhibiting the FAK phosphorylation activity and decreasing the viability of tumor cells

option for the treatment of patients with Enz resistance in the clinic.

Targeting MYO6 signaling suppresses EnzR tumor growth in vivo

To investigate whether the AR/MYO6/FAK signaling can be used as a therapeutic target for Enz-resistant PCa, we first established an in vivo mouse model in which 22Rv1 cells were implanted into male BALB/c nude mice to examine the effect of Y15 on Enz-resistant tumors. When the tumor volume reached 50 mm^3, the mice were randomly assigned to groups and injected (i.p.) with the control solvent (control), Enz (30 mg/kg), Y15 (5 mg/kg), or Enz (30 mg/kg)+Y15 (5 mg/kg) (combination) every other day for 3 weeks. Treatment with Enz alone had little effect on 22Rv1 cell growth, but Y15 alone significantly inhibited 22Rv1 cell growth compared to the vehicle (Fig. 6V–W); furthermore, treatment with Enz in combination with Y15 had a more significant inhibitory effect on 22Rv1 cell growth than treatment with Y15 or Enz alone (Fig. 6V–W). Tumor volume and weight also confirmed that treatment with Enz in combination with Y15 could significantly inhibit the growth of 22Rv1 cells compared with Y15 or Enz treatment alone (Fig. 6W–X), but mouse body weight did not change (Fig. 6Y). Additionally, IHC staining analysis of tumor xenografts revealed that the expression of Ki-67 and VEGFA was significantly lower in the Enz+Y15 combination treatment group than in the Enz or Y15 treatment alone group (Fig. 6Z). Taken together, these results indicate that both MYO6 knockdown and FAK inhibition can override Enz resistance in CRPC cells and that the combination of Enz and the FAK inhibitor Y15 can resensitize cells to Enz, thus effectively inhibiting the proliferation of Enz-resistant cells in vivo.

Discussion

Accumulating evidence suggests that therapeutic regimens targeting AR are valid for patients with advanced PCa, even for those who are diagnosed with CRPC. Although several assumptions support that the molecular mechanism underlying CRPC progression in the patients receiving ADT regimens involves aberrant AR signaling reactivation [1, 31], the exact mechanisms involved in the progression of ADT resistance, especially in patients receiving potent next-generation Enz, have not been fully elucidated. Approximately 80% of patients with CRPC exhibit marked AR overexpression at the mRNA and protein levels [32]. Transcription factors such as aldo-keto reductase family 1 member C3 (AKR1C3) might promote the development of Enz resistance by enhancing cellular androgen amplification [33], and glucocorticoid receptor (GR) might also contribute to the Enz resistance by

directly activating cellular survival pathways without the presence of AR [34]. Point mutations of AR also contribute to the potency of agonists, such as the AR-F877L and AR-F876L mutations that convert Enz to an agonist [35, 36]. In addition, targeting genes that are activated by AR is thought to be a potential therapeutic regimen for Enz-resistant CRPC [20]. Thus, reevaluating the significance of the clinical development of novel agents for patients who have failed Enz treatment is necessary.

Several previous potent next-generation inhibitors targeting AR in CRPC have been explored in clinical or preclinical studies. These effective inhibitors include AR antagonists, such as Enz, rezvilutamide, darolutamide, and apalutamide as well as the androgen synthesis inhibitor abiraterone [37]. Of these inhibitors, only abiraterone and Enz are effective against CRPC, and the others have limited efficacy against hormone-sensitive PCa (HSPC); moreover, most patients develop drug resistance over time, even though these medications significantly improve overall survival in patients with PCa [38, 39]. As a ubiquitously expressed unconventional myosin, MYO6 has also been shown to play a key role in PCa. Recent studies have shown that the MYO6 protein is associated with more aggressive histological features in PCa and that knockdown of MYO6 expression by siRNA results in the suppression of in vitro tumor cell migration and soft-agar colony formation [19]. However, the exact molecular mechanism by which MYO6 expression regulates CRPC progression and Enz resistance has not been determined.

In this study, we suggest that targeting MYO6 is a valid option for overcoming Enz-resistant CRPC. First, through analysis of public databases, it was observed that MYO6 expression was elevated in PCa tissues and was positively correlated with Gleason scores. Second, analysis of clinical samples from our center revealed that the mRNA and protein expression levels of MYO6 were upregulated in PCa tissues. Pancancer analysis revealed that the level of MYO6 expression in PCa and breast cancer tissues was higher than that in other types of cancer, indicating that MYO6 may be regulated by hormones. Sunniva et al. [40] reported that MYO6 expression is higher in patients with estrogen receptor (ER)-positive breast cancer than in patients with ER-negative breast cancer. Therefore, we assumed that MYO6 might also be involved in similar biological processes in PCa. Intriguingly, in the present study, the MYO6 expression level was greater in Enz-resistant C4-2 cells than in Enz-sensitive C4-2 cells, as was the expression of AR. MYO6 expression was investigated in AR^+/AR^- cell lines, and the results indicated that MYO6 expression was significantly greater in AR^+ cell lines (22Rv1, LNCaP, C4-2, and C4-2B) than in AR^- cell lines (DU145 and PC-3). By constructing cell lines stably overexpressing AR and stimulating the cells with DHT, we also confirmed that *MYO6* is probably a testosterone specifically regulatory gene. In addition, the expression of MYO6 was inhibited by Enz treatment in Enz-sensitive C4-2 cells. Furthermore, we verified the mechanism through which AR regulates MYO6 via ChIP-qPCR and dual-luciferase analysis, and the results confirmed that AR activated MYO6 at the transcriptional level and that DHT enhanced this process.

Also, we investigated how MYO6 acts in Enz-resistant cells and we found that the focal adhesion signaling was regulated by MYO6 through RNA-seq analysis. Kumar et al. [28] reported that suppressing ITGB8 downregulates the mRNA level of FAK. In addition, FAK, a key factor of the focal adhesion pathway, exhibited no significant difference in the mRNA and protein levels in our study. Therefore, we speculate that there are other signaling/pathways that mediate the regulatory effect of MYO6 on FAK function. Previous results showed that MYO1E, a member of the myosin family, promotes FAK phosphorylation at Y397 via its specific SH3 domain [27]. We assumed that MYO6 might also affect the level of FAK phosphorylation at Y397 in a similar way, thus altering the FAK activity. In this study, we found that the phosphorylation level of the FAK protein at Y397 (pFAK-Y397) was downregulated when MYO6 was knocked down, whereas MYO6 overexpression enhanced the pFAK-Y397 level in the Enz-resistant PCa cells. Moreover, we observed that ITGB8 expression increased in C4-2R cells, whereas ITGB8 expression decreased in C4-2R-shMYO6 cells compared to C4-2R cells; and the main interacting amino acids were glutamic acid on ITGB8 and arginine on FAK, which was confirmed by the protein molecular docking result. These findings indicate that MYO6 activates the phosphorylation of FAK at residue-Y397 by the positive modulation of ITGB8 in Enz-resistant PCa cells, thus enhancing FAK activity.

In the present study, we investigated the important role of MYO6 in AR overexpression-related Enz resistance. We found that Enz resistance was reversed by MYO6 knockdown in 22Rv1 and C4-2R cells and that MYO6 silencing enhanced the inhibitory effect of Enz on cell proliferation not only of Enz-sensitive PCa cell lines but also of Enz-resistant PCa cell lines. Furthermore, we suggest that MYO6 enhances Enz resistance by accumulating FAK phosphorylated at Y397. Y15, a specific inhibitor that targets the Y397 site [29], sensitizes PCa cells to Enz both in vitro and in vivo, indicating that combination treatment with Enz and Y15 could be a potential option for CRPC treatment. But some problems need further study. First, high MYO6 expression correlates with high AR expression and AR effects MYO6 transcription. Conversely, the effect of MYO6 on AR needs also be investigated. Second, whether other inhibitors targeting androgen/AR signaling, such as abiraterone,

apalutamide, rezvilutamide, and darolutamide, etc., have similar effects needs to further be studied to explore the detailed mechanism of action of these drugs. Finally, any limitations on targeting MYO6, this important protein (e.g. in drug development), that may justify targeting FAK and raise concerns on directly targeting MYO6 need be fully evaluated and discussed.

In summary, our study identified a specific signal transduction pathway, the AR/MYO6/FAK axis, in Enz-resistant PCa cells. Targeting this axis could effectively circumvent Enz resistance, and Enz combined with Y15 could be a novel and effective therapeutic approach for CRPC (Fig. 7).

Supplementary Information

The online version contains supplementary material available at https://doi.org/10.1186/s12964-024-01897-z.

Supplementary Material 1

Supplementary Material 2

Acknowledgements
This study was supported by the National Natural Science Foundation of China (82303856, 81671318, 82172741), the Shanghai Sailing Program (20YF1443800), and the China Anti-cancer Association Foundation (YJQN202201).

Author contributions
Ye D., Hong Z., Lin G., and Hong Z-Y. designed and supervised the experiments and contributed to funding acquisition. Zheng S., Tan Y., Wang Y., Ma T., and Zhang Z. performed the experiments and analyzed the data. Zheng S., Hong Z., and Tan Y. contributed to clinical sample collection. Zheng S. and Li J. wrote the manuscript. Hong Z-Y., Hong Z. and Ye D. reviewed and edited the manuscript. All authors read and approved the final manuscript.

Data availability
No datasets were generated or analysed during the current study.

Declarations

Conflict of interest
The authors declare no competing financial interests.

Author details
[1]Department of Urology, Fudan University Shanghai Cancer Center, Shanghai 200032, China
[2]Department of Oncology, Shanghai Medical College, Fudan University, Shanghai 200032, China
[3]Shanghai Genitourinary Cancer Institute, Shanghai 200032, China
[4]Department of Nursing Administration, Shanghai Cancer Center, Fudan University, Shanghai 200032, China
[5]Department of Pharmacology and Laboratory of Quantitative Pharmacology, Wannan Medical College, Wuhu, Anhui 241000, China
[6]Qingdao Institute, School of Life Medicine, Department of Urology, Fudan University Shanghai Cancer Center, Fudan University, Qingdao, China

Received: 18 June 2024 / Accepted: 18 October 2024
Published online: 24 October 2024

References

1. Feng FY, Thomas S, Saad F, Gormley M, Yu MK, Ricci DS, Rooney B, Brookman-May S, McCarthy S, Olmos D, et al. Association of Molecular Subtypes with Differential Outcome to Apalutamide Treatment in Nonmetastatic Castration-resistant prostate Cancer. JAMA Oncol. 2021;7(7):1005–14.
2. Yu EY, Kolinsky MP, Berry WR, Retz M, Mourey L, Piulats JM, Appleman LJ, Romano E, Gravis G, Gurney H, et al. Pembrolizumab Plus Docetaxel and Prednisone in patients with metastatic castration-resistant prostate Cancer: long-term results from the phase 1b/2 KEYNOTE-365 cohort B study. Eur Urol. 2022;82(1):22–30.
3. Hoffman-Censits J, Kelly WK. Enzalutamide: a novel antiandrogen for patients with castrate-resistant prostate cancer. Clin Cancer Res. 2013;19(6):1335–9.
4. Ma B, Fan Y, Zhang D, Wei Y, Jian Y, Liu D, Wang Z, Gao Y, Ma J, Chen Y, et al. De Novo Design of an androgen receptor DNA binding domain-targeted peptide PROTAC for prostate Cancer therapy. Adv Sci (Weinh). 2022;9(28):e2201859.
5. Wasmuth EV, Broeck AV, LaClair JR, Hoover EA, Lawrence KE, Paknejad N, Pappas K, Matthies D, Wang B, Feng W, et al. Allosteric interactions prime androgen receptor dimerization and activation. Mol Cell. 2022;82(11):2021–31. e5.
6. Sawant M, Mahajan K, Renganathan A, Weimholt C, Luo J, Kukshal V, Jez JM, Jeon MS, Zhang B, Li T, et al. Chronologically modified androgen receptor in recurrent castration-resistant prostate cancer and its therapeutic targeting. Sci Transl Med. 2022;14(649):eabg4132.
7. Senapati D, Kumari S, Heemers HV. Androgen receptor co-regulation in prostate cancer. Asian J Urol. 2020;7(3):219–32.
8. Hamid AA, Gray KP, Shaw G, MacConaill LE, Evan C, Bernard B, Loda M, Corcoran NM, Van Allen EM, Choudhury AD, et al. Compound genomic alterations of TP53, PTEN, and RB1 tumor suppressors in localized and metastatic prostate Cancer. Eur Urol. 2019;76(1):89–97.
9. Rodriguez Y, Unno K, Truica MI, Chalmers ZR, Yoo YA, Vatapalli R, Sagar V, Yu J, Lysy B, Hussain M, et al. A genome-wide CRISPR activation screen identifies PRRX2 as a Regulator of Enzalutamide Resistance in prostate Cancer. Cancer Res. 2022;82(11):2110–23.
10. Wang Y, Chen J, Wu Z, Ding W, Gao S, Gao Y, Xu C. Mechanisms of enzalutamide resistance in castration-resistant prostate cancer and therapeutic strategies to overcome it. Br J Pharmacol. 2021;178(2):239–61.
11. Ouyang Z, Zhao S, Yao S, Wang J, Cui Y, Wei K, Jiu Y. Multifaceted function of Myosin-18, an unconventional class of the myosin superfamily. Front Cell Dev Biol. 2021;9:632445.
12. Sellers JR. Myosins: a diverse superfamily. Biochim Biophys Acta. 2000;1496(1):3–22.
13. Fili N, Hari-Gupta Y, Dos Santos A, Cook A, Poland S, Ameer-Beg SM, Parsons M, Toseland CP. NDP52 activates nuclear myosin VI to enhance RNA polymerase II transcription. Nat Commun. 2017;8(1):1871.
14. Yoshida H, Cheng W, Hung J, Montell D, Geisbrecht E, Rosen D, Liu J, Naora H. Lessons from border cell migration in the Drosophila ovary: a role for myosin VI in dissemination of human ovarian cancer. Proc Natl Acad Sci U S A. 2004;101(21):8144–9.
15. Cho SJ, Chen X. Myosin VI is differentially regulated by DNA damage in p53- and cell type-dependent manners. J Biol Chem. 2010;285(35):27159–66.
16. Wang H, Wang B, Zhu W, Yang Z. Lentivirus-mediated knockdown of myosin VI inhibits cell proliferation of breast Cancer cell. Cancer Biother Radiopharm. 2015;30(8):330–5.
17. Puri C, Chibalina MV, Arden SD, Kruppa AJ, Kendrick-Jones J, Buss F. Overexpression of myosin VI in prostate cancer cells enhances PSA and VEGF secretion, but has no effect on endocytosis. Oncogene. 2010;29(2):188–200.
18. Dunn TA, Chen S, Faith DA, Hicks JL, Platz EA, Chen Y, Ewing CM, Sauvageot J, Isaacs WB, De Marzo AM, et al. A novel role of myosin VI in human prostate cancer. Am J Pathol. 2006;169(5):1843–54.
19. Wang D, Zhu L, Liao M, Zeng T, Zhuo W, Yang S, Wu W. MYO6 knockdown inhibits the growth and induces the apoptosis of prostate cancer cells by decreasing the phosphorylation of ERK1/2 and PRAS40. Oncol Rep. 2016;36(3):1285–92.
20. Wang K, Luo J, Yeh S, You B, Meng J, Chang P, Niu Y, Li G, Lu C, Zhu Y, et al. The MAO inhibitors phenelzine and clorgyline revert enzalutamide resistance in castration resistant prostate cancer. Nat Commun. 2020;11(1):2689.
21. Moffat J, Grueneberg DA, Yang X, Kim SY, Kloepfer AM, Hinkle G, Piqani B, Eisenhaure TM, Luo B, Grenier JK, et al. A lentiviral RNAi library for human and mouse genes applied to an arrayed viral high-content screen. Cell. 2006;124(6):1283–98.
22. Langmead B, Salzberg SL. Fast gapped-read alignment with Bowtie 2. Nat Methods. 2012;9(4):357–9.

23. Jinesh GG, Brohl AS. Classical epithelial-mesenchymal transition (EMT) and alternative cell death process-driven blebbishield metastatic-witch (BMW) pathways to cancer metastasis. Signal Transduct Target Ther. 2022;7(1):296.
24. Kohli J, Ge C, Fitsiou E, Doepner M, Brandenburg SM, Faller WJ, Ridky TW, Demaria M. Targeting anti-apoptotic pathways eliminates senescent melanocytes and leads to nevi regression. Nat Commun. 2022;13(1):7923.
25. Zhou Z, Yang R, Dong J, Di Y, Yang Y, Huang Y, Yang X, Liu W, Wang J, Liu P, et al. Pore forming-mediated intracellular protein delivery for enhanced cancer immunotherapy. Sci Adv. 2022;8(46):eabq4659.
26. Armstrong AJ, Szmulewitz RZ, Petrylak DP, Holzbeierlein J, Villers A, Azad A, Alcaraz A, Alekseev B, Iguchi T, Shore ND, et al. ARCHES: a Randomized, Phase III Study of Androgen Deprivation Therapy with Enzalutamide or Placebo in Men with metastatic hormone-sensitive prostate Cancer. J Clin Oncol. 2019;37(32):2974–86.
27. Heim JB, Squirewell EJ, Neu A, Zocher G, Sominidi-Damodaran S, Wyles SP, Nikolova E, Behrendt N, Saunte DM, Lock-Andersen J, et al. Myosin-1E interacts with FAK proline-rich region 1 to induce fibronectin-type matrix. Proc Natl Acad Sci U S A. 2017;114(15):3933–38.
28. Kumar V, Soni UK, Maurya VK, Singh K, Jha RK. Integrin beta8 (ITGB8) activates VAV-RAC1 signaling via FAK in the acquisition of endometrial epithelial cell receptivity for blastocyst implantation. Sci Rep. 2017;7(1):1885.
29. Golubovskaya VM, Figel S, Ho BT, Johnson CP, Yemma M, Huang G, Zheng M, Nyberg C, Magis A, Ostrov DA, et al. A small molecule focal adhesion kinase (FAK) inhibitor, targeting Y397 site: 1-(2-hydroxyethyl)-3, 5, 7-triaza-1-azoniatricyclo [3.3.1.1(3,7)]decane; bromide effectively inhibits FAK autophosphorylation activity and decreases cancer cell viability, clonogenicity and tumor growth in vivo. Carcinogenesis. 2012;33(5):1004–13.
30. Steinestel K, Trautmann M, Jansen EP, Dirksen U, Rehkamper J, Mikesch JH, Gerke JS, Orth MF, Sannino G, Arteaga MF, et al. Focal adhesion kinase confers pro-migratory and antiapoptotic properties and is a potential therapeutic target in ewing sarcoma. Mol Oncol. 2020;14(2):248–60.
31. Kishan AU, Steigler A, Denham JW, Zapatero A, Guerrero A, Joseph D, Maldonado X, Wong JK, Stish BJ, Dess RT, et al. Interplay between duration of Androgen Deprivation Therapy and External Beam Radiotherapy with or without a Brachytherapy Boost for Optimal Treatment of High-risk prostate Cancer: a patient-Level Data Analysis of 3 cohorts. JAMA Oncol. 2022;8(3):e216871.
32. Jernberg E, Bergh A, Wikstrom P. Clinical relevance of androgen receptor alterations in prostate cancer. Endocr Connect. 2017;6(8):R146–61.
33. Verma K, Gupta N, Zang T, Wangtrakluldee P, Srivastava SK, Penning TM, Trippier PC. AKR1C3 inhibitor KV-37 exhibits Antineoplastic effects and potentiates Enzalutamide in Combination Therapy in prostate adenocarcinoma cells. Mol Cancer Ther. 2018;17(9):1833–45.
34. Li J, Alyamani M, Zhang A, Chang KH, Berk M, Li Z, Zhu Z, Petro M, Magi-Galluzzi C, Taplin ME et al. Aberrant corticosteroid metabolism in tumor cells enables GR takeover in enzalutamide resistant prostate cancer. Elife. 2017;6(.
35. Joseph JD, Lu N, Qian J, Sensintaffar J, Shao G, Brigham D, Moon M, Maneval EC, Chen I, Darimont B, et al. A clinically relevant androgen receptor mutation confers resistance to second-generation antiandrogens enzalutamide and ARN-509. Cancer Discov. 2013;3(9):1020–9.
36. Montgomery RB, Mostaghel EA, Vessella R, Hess DL, Kalhorn TF, Higano CS, True LD, Nelson PS. Maintenance of intratumoral androgens in metastatic prostate cancer: a mechanism for castration-resistant tumor growth. Cancer Res. 2008;68(11):4447–54.
37. Mori K, Mostafaei H, Pradere B, Motlagh RS, Quhal F, Laukhtina E, Schuettfort VM, Abufaraj M, Karakiewicz PI, Kimura T, et al. Apalutamide, enzalutamide, and darolutamide for non-metastatic castration-resistant prostate cancer: a systematic review and network meta-analysis. Int J Clin Oncol. 2020;25(11):1892–900.
38. Drago JZ, Gonen M, Thanarajasingam G, Sacks CA, Morris MJ, Kantoff PW, Stopsack KH. Inferences about drug safety in phase III trials in Oncology: examples from advanced prostate Cancer. J Natl Cancer Inst. 2021;113(5):553–61.
39. Halabi S, Jiang S, Terasawa E, Garcia-Horton V, Ayyagari R, Waldeck AR, Shore N. Indirect comparison of Darolutamide versus Apalutamide and Enzalutamide for Nonmetastatic Castration-resistant prostate Cancer. J Urol. 2021;206(2):298–307.
40. Bjorklund SS, Panda A, Kumar S, Seiler M, Robinson D, Gheeya J, Yao M, Alnaes GIG, Toppmeyer D, Riis M, et al. Widespread alternative exon usage in clinically distinct subtypes of Invasive Ductal Carcinoma. Sci Rep. 2017;7(1):5568.

Publisher's note

Springer Nature remains neutral with regard to jurisdictional claims in published maps and institutional affiliations.